J|A|C|S
ARTICLES
Published on Web 02/04/2004

Pyridinedicarboxamide Strands Form Double Helices via an Activated Slippage Mechanism

Angela Acocella,[†,‡] Alessandro Venturini,*[,†] and Francesco Zerbetto*[,‡]

Contribution from the ISOF, Consiglio Nazionale delle Ricerche, via Gobetti 101, 40129 Bologna, Italy, and Dipartimento di Chimica "G. Ciamician", Università di Bologna, V. F. Selmi 2, 40126, Bologna, Italy

Received August 25, 2003; E-mail: A.Venturini@isof.cnr.it; francesco.zerbetto@unibo.it

Abstract: The intertwining process of two strands of oligo-pyridinecarboxamides to form a double helix (*Nature* **2000**, *407*, 720) is found to consist of a series of discrete steps, where the tail of one of the strands proceeds inside the other single helix in an eddy-like process. While a plethora of minima can be located along the pathway, they exist only for a few, well-defined supramolecular arrangements of the two molecules. The initial transition state for the introduction of one molecule in the pitch of the other has the largest barrier and is therefore the rate-determining step of an activated slippage mechanism, which is characterized by a series of roller-coasting hills. Along the entire pathway, the intramolecular energy that stabilizes the single helices is slowly transformed into intermolecular energy that finally provides the necessary stabilization only near the end of the entwining process. Solvent or other chemical factors, such as the presence of ions, able to destabilize the full formation of the double helix may therefore drastically affect its formation.

Introduction

The dynamics of foldamers[1] and the investigation of molecular-level double helix formation are prime examples of the complexity of supra-molecular interactions. A new versatile set of cases for single- and double-helix formation is the family of oligo-pyridinedicarboxamide strands.[2] These molecules have a remarkable propensity for the creation of reversible equilibria between single and double helices as a function of concentration, solvent, temperature, and water impurities. The mechanistic details of the interconversion are, to a good extent, unknown. Their knowledge could play a crucial role in the tuning, or even the improvement, of the original architecture to produce systems with a varying degree of similarity to DNA analogues.

After their discovery,[2] the behavior of the two types of helices was thoroughly studied by NMR and X-ray structural investigations that were able to shed light also on some aspects of their interconversion.[3] Concurrent molecular dynamics simulations showed that, at high temperatures, the double helix of relatively short, pentameric strands is destroyed by the progressive unfolding of the individual chains.

At any temperature, the reversible folding−unfolding mechanism is governed by the (activation) free energy. However, at temperatures close to room temperature, RT, the mechanism may substantially differ from that found at high temperatures where the entropic contribution, $T\Delta S$, dominates. Indeed, the process must be controlled by the enthalpic term, which is closely associated to the minimum energy pathway that links the adduct formed by two abutting single helices to the perfectly intertwined duplex. This mechanical path leads, at the same time, both to the assembly and to the disassembly of the double helix.

Here, we investigate the potential energy surface, PES, for the assembly mechanism of the double helix of the heptamer of pyridine dicarboxamide, 7-PDCA (Scheme 1). We characterize several minima along the pathway of intertwining of the two strands and calculate their free energy. From the analysis, we infer that the rate-determining step for the formation of the duplex must occur at an early stage of the interaction. The identification of the critical transition states confirms the picture that emerges from the study of the plethora of minima that exist for the interaction of the two chains.

Methodology

All of the molecular structures, intermediates, and transition states, were fully optimized using a full matrix Newton Rapson algorithm (FMNR) within the OPLS-AA[4] molecular mechanics procedure as implemented in the Macromodel program.[5] Convergence to the stationary point was obtained when the RMS of the gradient was less than 0.01 kJ/Å-mol. The initial inputs to locate the stationary points, i.e., minima and transition states, of the potential energy surface, PES, were obtained by rigid mechanical rotation of one of the strands accompanied by its displacement, which effectively results in disentangling the two chains.

[†] ISOF.
[‡] Dipartimento di Chimica "G. Ciamician", Università di Bologna.

(1) (a) Hill, D. J.; Mio, M. J.; Prince, R. B.; Hughes, T. H.; Moore, J. S. *Chem. Rev.* **2001**, *101*, 3893−4011. (b) Gellman, S. H. *Acc. Chem. Res.* **1998**, *31*, 173−180.
(2) Berl, V.; Huc, I.; Khoury, R. G.; Krische, M. J.; Lehn, J.-M. *Nature* **2000**, *407*, 720.
(3) (a) Berl, V.; Huc, I.; Khoury, R. G.; Krische, M. J.; Lehn, J.-M. *Chem. Eur. J.* **2001**, *7*, 2798. (b) Berl, V.; Huc, I.; Khoury, R. G.; Krische, M. J.; Lehn, J.-M. *Chem. Eur. J.* **2001**, *7*, 2810.
(4) Jorgensen, W. L.; Maxwell, D. S.; Tirado-Rives, J. *J. Am Chem. Soc.* **1996**, *118*, 11 255.
(5) Mohamadi, F.; Richards, N. G. J.; Guida, W. C.; Liskamp, R.; Lipton, M.; Caufield, C.; Chang, G.; Hendrickson, T.; Still, W. C. *J. Comput. Chem.* **1990**, *11*, 440−467.

10.1021/ja038103f CCC: $27.50

Scheme 1

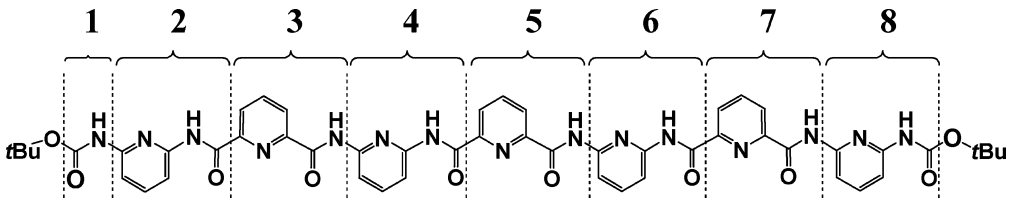

The presence of the $CHCl_3$ solvent was simulated using the GB/SA implicit solvent model,[5] which has found a variety of applications for chloroform[6d−6i] and has also been extended to study organic solvent interactions with quantum chemical methods.[6j,6k]

Free energies, ΔG_{298}, were calculated using the $\Delta G_{298} = E(MM+) - RT \ln Q$ equation where Q is the partition function, calculated in the harmonic approximation, which seems adequate for systems of this size.[7] The nonbonded energy contributions were separated in inter- and intrafragment: $\Delta E_{tot}(\text{nonbonded}) = \Delta E_{inter}(\text{nonbonded}) + \Delta E_{intra}(\text{nonbonded})$.

The minima at each side of the transition states were identified by relaxing their structures and locating the closest complexes.

Results and Discussion

When a host of weakly bonding interactions, typically π-stacks and/or H-bonds, control (supra)molecular structure and dynamics, parameters external to the molecules may readily alter the preferred pathways followed by the system. Oligo-pyridinedicarboxamide constitute a prime example of this behavior and their ordered aggregation in double helices critically depends on the environment.[1,2] Apart from the high-temperature entropic contribution mentioned above, Boltzmann distribution may wreak havoc on the structural stability, as a simple textbook example can illustrate: for a pair of molecules bound by 5 kcal mol^{-1}, the number of duplexes dissociated at RT is slightly more than 10^{-4}, if the temperature is increased to 700 °C, the dissociation is augmented by a factor of about 300. This consideration sets some limits to the validity of our computational investigation of the potential energy surface, PES, of 2(7-PDCA) $\rightleftarrows$ $(7\text{-PDCA})_2$, which, while it may not be relevant for the self-assembly $\rightleftarrows$ disassembly at high temperatures, holds when the thermal motions can effectively disrupt only one weakly bonding interaction at a time.

Figure 1 compares the X-ray and the calculated structures of the single and double helices of the molecule shown in Scheme 1 (notice that the same molecule was 3 in ref 2 and 2 in ref 3b). The experimental structure is obtained in the crystal, where solvent molecules are also present; the calculations are for molecules embedded in $CHCl_3$ simulated by a continuum model. Some differences are expected; for instance, in the solid the bottom of the double helix pinches a nitrobenzene, a feature

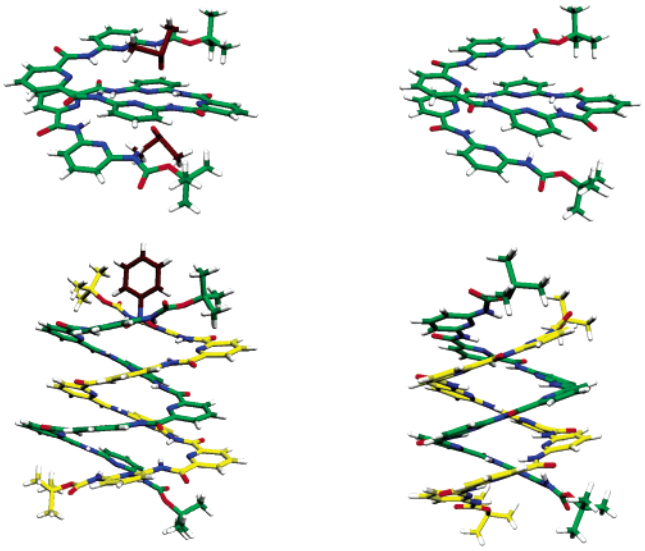

Figure 1. Comparison of X-ray and calculated structures of single and double helices of 7-PDCA: top left, X-ray structure of the single helix; top right, calculated structure of the single helix top left; bottom left, X-ray structure of the double helix; bottom right, calculated structure of the double helix. The two strands are identical and have different colors to assist the eye. In the X-ray structures solvent molecules are present (nitrobenzene and dimethylsulfoxide in double and single helices respectively).

absent in the calculations. Analogously, the NH···O hydrogen bonds with water molecules present in the experimental structure of the duplex are here absent. In general, one would expect that the insertion of solvent molecules and the pull of the nearby strands of the crystal may form a slightly more open structure. Importantly, however, the completion of a single helical turn requires 4(4.5) pyridines in the duplex(single helix) both in the solid and in the simulations.

The details of the energy and the structural characterization and the minima and transition states for the double helix formation are given in Tables 1−4 and Figures 2 and 3. Table 1 presents the (free) energies of the various structures together with their nonbonding components, Table 2 gives the $\pi-\pi$ stacks, Tables 3 and 4 the hydrogen bonds. Both inter- and intrastrand nonbonding interactions are given, although most of the discussion is focused on the interchain contacts. The numbering of the individual fragments is shown in Scheme 1; if the fragment is on the first strand, it has no prime, if it is part of the second strand it is identified by a prime. Either one, or two, NH···N hydrogen bonds can be formed between the individual fragments.

Cursory Exam. Stable structures are labeled alphabetically **A** to **N**, whereas the transition states are called **TS*n***, with n = 1, 2,...6. Both minima and transition states are ordered sequentially as the formation of the duplex proceeds. The second column of Table 1 presents the relative energies during the

(6) (a) Still, W. C.; Tempczyk, A.; Hawley, R. C.; Hendrickson, T. F. *J. Am. Chem. Soc.* **1990**, *112*, 6127−6129. (b) Hasel, W.; Hendrickson, T. F.; Still, W. C. *Tetrahedron Comput. Method* **1988**, *1*, 103. (c) Viswanadhan, V. N.; Mcdonald, D. Q.; Still, W. C. *J. Comput. Chem.* **1998**, *19*, 769−780. (d) Nevins, N.; Cicero, D.; Snyder, J. P. *J. Org. Chem.* **1999**, *64*, 3979−3986. (e) Grabuleda, X.; Jaime, C. *J. Org. Chem.* **1998**, *63*, 9635−9643. (f) Luo, R.; Head, M. S.; Given, J. A.; Gilson, M. K. *Biophys. Chem.* **1999**, *78*, 183−193. (g) Barnett-Norris, J.; Guarnieri, F.; Hurst, D. P.; Reggio, P. H. *J. Med. Chem.* **1998**, *41*, 4861−4872. (h) Senderowitz, H.; McDonald, D. Q.; Still, W. C. *J. Org. Chem.* **1997**, *62*, 9123−9127. (i) Williams, D. J.; Hall, K. B. *J. Phys. Chem.* **1996**, *100*, 8224−8229. (j) Giesen, D. J.; Hawkins, G. D.; Liotard, D. A.; Cramer, C. J.; Truhlar, D. G. *Theor. Chem. Acc.* **1997**, *98*, 85−109. (k) Giesen, D. J.; Chambers, C. C.; Cramer, C. J.; Truhlar, D. G. *J. Phys. Chem. B* **1997**, *101*, 2061−2069.
(7) Leigh, D. A.; Murphy, A.; Smart, J. P.; Deleuze, M. S.; Zerbetto, F. *J. Am. Chem. Soc.* **1998**, *120*, 6458−6467. (b) Deleuze, M. S.; Leigh, D. A.; Zerbetto, F. *J. Am. Chem. Soc.* **1999**, *121*, 2364−2379.

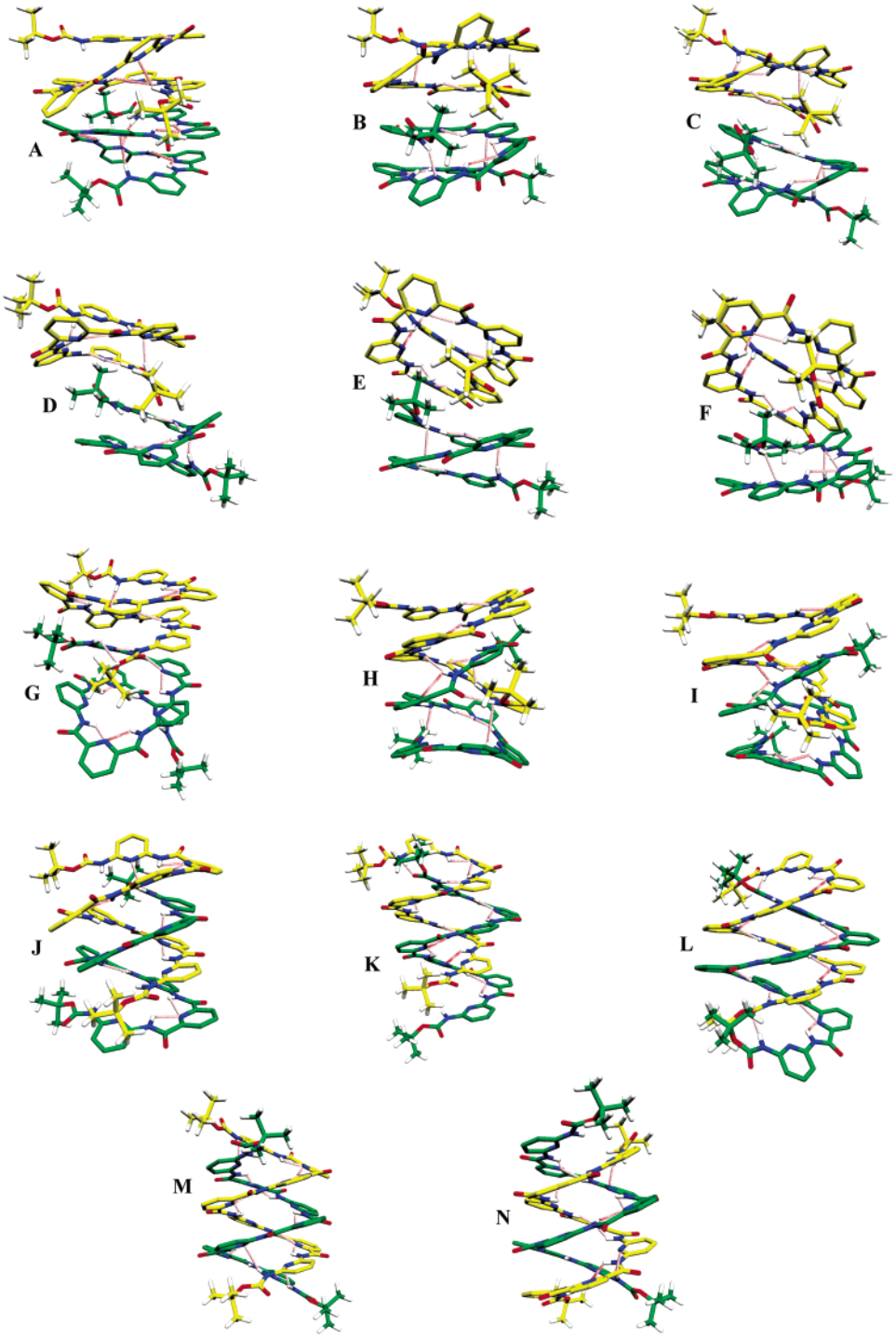

Figure 2. Minimum energy structures A−N encountered along the intertwining pathway. The two strands are identical and have different colors to assist the eye.

entwining process. While the trend of the total energy is smooth, the intrachain and interchain components of the energy go in leaps and bounds. This is caused by the discrete nature of the number of the H-bonds and π-stacks that are formed and that often is increased, or decreased, by several units between two adjacent points, see Tables 2−4.

A very large number of similar structures can be located for a few selected types of minima that correspond to (i) contact, (ii) half-turn screw-in, (iii) one and a half-turn, and (iv) double helix. Attempts to locate other intermediate adducts failed systematically. Overall, the entwining process is describable as a series of subsequent, discrete eddy-like steps, where the tail of a strand creeps inside the other single helix.

Before Intertwining. In solution, if the strand concentration is sufficient, dimerization of two single helices occurs. Back-to-back contact is the configuration that initiates double helix formation. A side-by-side interpenetrated pair is also possible in an arrangement that brings to mind a "failed" double helix. In 7-PDCA, the back-to-back and side-by-side adducts are almost equi-energetic. The most stable back-to-back complex, **A**, is favored by 0.5 kcal mol^{-1} on the basis of the energy, but the side-by-side adduct has a free energy lower by

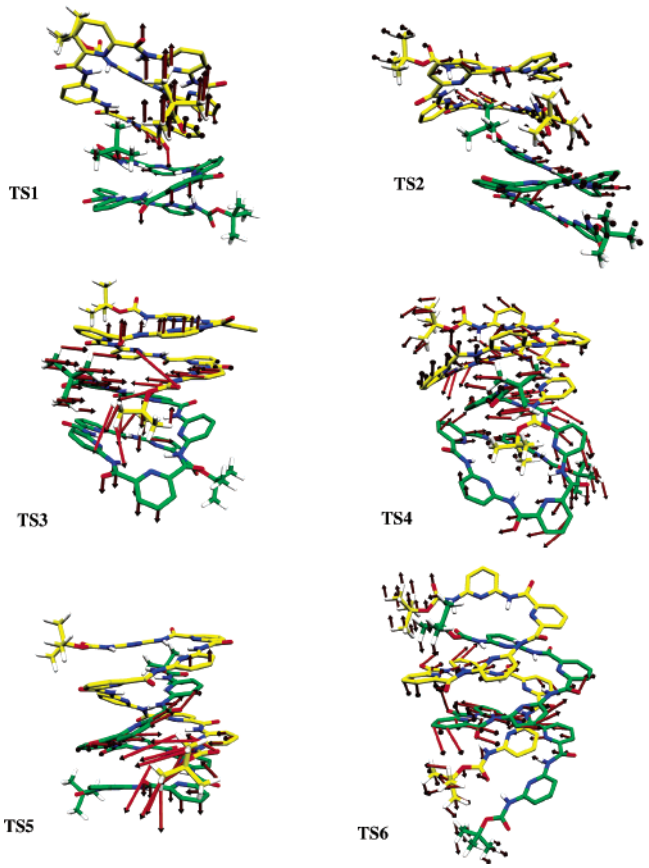

Figure 3. Transition state structures encountered along the intertwining pathway. The arrows represent the atomic motion that leads to one of the two minima located at bottom of the hill of the transition state; (a) **TS1**, (b) **TS2**, (c) **TS3**, (d) **TS4**, (e) **TS5**, and (f) **TS6**. The two strands are identical and have different colors to assist the eye.

Table 1. Energy, Free Energy, and Non-Bonded Interactions (NB), kcal mol^{-1}, of the Stationary Points of the Potential Energy Surface of the Double Helix Formation of 7-PDCA

structures	ΔE	$\Delta\Delta G_{tot}$	ΔE_{strain}	ΔE_{tot} NB	ΔE_{inter} NB	ΔE_{intra} NB	$\Delta E_{solvation}$
A	0.0	0.0	0.0	0.0	0.0	0.0	0.0
B	0.9	0.7	1.1	0.6	6.1	−5.5	−0.8
C	3.2	2.8	3.0	3.2	12.5	−9.3	−3.0
D	3.1	1.2	1.9	5.8	13.9	−8.0	−4.6
E	4.8	2.3	2.4	3.4	8.9	−5.5	−1.1
F	2.9	−0.8	4.6	2.1	9.1	−7.0	−3.7
G	3.5	3.5	2.2	5.7	−4.2	10.0	−4.4
H	2.9	−0.8	10.9	−4.1	−27.1	23.0	−3.9
I	−0.3	−3.3	5.3	−6.6	−25.9	19.2	1.1
J	−5.1	−6.0	2.5	−8.7	−61.5	52.8	1.1
K	−2.2	−6.8	18.5	−16.7	−63.0	46.4	−4.0
L	−11.9	−13.2	11.0	−19.1	−69.1	50.0	−3.8
M	−13.9	−18.4	6.7	−20.7	−76.6	55.8	0.1
N	−13.9	−19.9	4.8	−19.5	−76.8	57.2	0.8
TS1	8.2	1.2	4.4	6.3	12.9	−6.7	−2.5
TS2	8.2	7.4	1.6	12.3	18.4	−6.1	−5.7
TS3	12.9	9.5	3.6	12.8	5.6	7.2	−3.6
TS4	5.4	2.4	6.5	1.7	−12.1	13.8	−2.7
TS5	10.7	6.1	2.7	14.3	−24.7	39.0	−6.3
TS6	−2.1	−5.2	7.7	−3.8	−55.5	51.7	−7.2

0.7 kcal mol^{-1}. In consideration of their similar stability, and of the fact that the side-by-side arrangement is difficult, or impossible, to attain when alkyl chain are attached to the pyridyl moieties (these derivatives also form double helices,[1,2]) in the following the lateral arrangement will not be further considered.

Table 2. List of the Inter- and Intrastrands $\pi-\pi$ Stacks for the Stationary Points of the Potential Energy Surface of the Double Helix Formation of 7-PDCA[a]

structure	$\pi-\pi_{inter}$	$\pi-\pi_{intra}$
A	**7−2′**; **8−3′**	**2−7**; **3−8**; **2′−7′**
B	**2−6′**; **7−3′**	**2−7**; **3′−8′**
C	**7−3′**	**2−7**; **3−8**; **3′−8′**
D	**7−2′**	**2−7**; **3−8**; **2′−7′**; **3′−8′**
E	**7−2′**	**2−7**; **2′−7′**; **3′−8′**
F	**7−2′**	**2−7**; **3−8**; **2′−7′**; **3′−8′**
G	**7−3′**	**2−7**; **3−8**; **3′−8′**
H	6−3′; 3′−6; **2′−3**	**2−6**; **3′−8′**
I	5−2′; 6−3′; 7−4′; 8−7′	**2−7**; **3′−8′**
J	**3−2′**-7−6′; **4−3′**−8−7′; 5−4′; 6−5′	
K	**3−3′**-7−7′; 4−4′−8′; 5−5′; 6−6′−**2−2′**;	
L	2−6′−3−7′; 3−3′−7−7′; 4−4′−8; 5−5′	
M	**2−3′**-6−7′; 3−4′−7−8′; 4−5′−8; 2′−5−6′	
N	2−3′−6−7′; 2−5′−6; 3−4′−7; 4−5′−8	
TS1	**7−3′**;**8−5′**	**2−7**; **3−8**; **2′−7′**; **3′−8′**
TS2		**2−7**; **3−8**; **2′−7′**; **3′−8′**
TS3	**5−2′**; **8−4′**	**2−7**; **4−8**; **2′−7′**; **3′−8′**
TS4	5−2′; **8−4′**	**2−7**; **3′−8′**
TS5	**2−6−4′**; 5−3′; **6−4′**; **7−6′**; **8−6′**	**4′−8′**
TS6	2−2′−6−6′; 3−3′−7; 4−4′−8; 5−5′	

[a] Underlined, the stacks that intertwine the chains; in bold, the stacks that hold the duplex together but do not cause intertwining of the chains.

Table 3. List of the Interstrands NH···N and NH···O H-bonds for the Stationary Points of the Potential Energy Surface of the Double Helix Formation of 7-PDCA[a]

structure	NH···N$_{inter}$	NH···O$_{inter}$
A	**8−3′**	
B		**5−1′**
C		**4′-8**
D		**6−1′**; **7−1′**
E		**2′−7**; **3′−7**
F		**7−4′**; **7−5′**
G	**8−2′**; **8−2′**	**8−1′**
H	6−2′; 7−1′; 7−2′; 8−3′	**2−1′**; 7−5′; 8−2′
I	**4−1′**; **4−2′**; **6−2′**; 7−4′; 8−2′; 8−4′	
J	**1′−2**; **2−2′**; 3′−8; 5−4′; 6−2′; 6−4′; 7−6′; 8−4′; 8−6′; 8−8′	
K	1−5′; 2−4′; 2−4′; 2−5′; 5−4′; 5−8′; 6−8′; 6−8′; 7−8′	2−6′; 8−8′
L	2−2′; 3−2′; 4−1′; 8−6′; 8−6′; 8−7′;	**1−1′**; 8−5′; 8−8′
M	1−4′; **2−1′**; **2−2′**; 2−4′; 3−6′; 4−3′; 4−4′; 4−6′; 5−8′; 6−5′; 6−8′; 8−7′; 8−8′	
N	1−2′; 1−4′; 2−2′; 2−4′; 3−6′; 4−6′; 5−8′; 6−8′; 8−8′; 8′-6	
TS1		**7−4′**
TS2		**6−1′**; **7−1′**
TS3	**5−1′**	**7−3′**
TS4	**4−2′**; **4−2′**; 7−3′; **8−2′**; **8−2′**	
TS5	5−3′; 6−2′; 6−2′; 6−3′; 8−7′	6−4′
TS6	4−2′; 4−3′; 5−1′; 5−2′; 7−2′; 8−5′; 8−6′; 8−7′; 8−8′	

[a] Underlined the H-bonds that intertwine the chains, in bold the H-bonds that hold the duplex together but do not cause intertwining of the chains. The cutoff distance between heavy atoms for the hydrogen bond is 3.4 Å.

Fastening the Tails of Two Single Helices, Phase I, A−F. The lowest energy of the back-to-back structures, **A**, is taken as the zero of energy. The association produces some interchain

Table 4. List of the Intra-strands NH···N H-bonds for the Stationary Points of the Potential Energy Surface of the Double Helix Formation of 7-PDCA[a]

structure	$NH\cdots N_{intra}$
A	1−6; 2−6; 2−3; 3−3; 4−8; 3−8; 4−5; 5−5; 6−7; 7−7; 1′−6′; 4′−5′; 5′−5′; 4′−8′; 2′−6′; 6′−7′; 7′−7′; 2′−3′; 3′−3′
B	1−6; 2−6; 2−3; 3−3; 6−7; 7−7; 3−8; 4−8; 5−5; 4−5; 1′−6′; 2′−6′; 6′−7′; 7′−7′; 3′−8′; 4′−5′; 5′−5′; 2′−3′; 3′−3′; 4′−8′
C	1−6; 2−6; 2−3; 3−3; 3−8; 7−7; 6−7; 4−5; 5−5; 4−8; 3′−3′; 2′−3′; 3′−8′; 7′−7′; 6′−7′; 2′−6′; 4′−8′; 1′−6′; 5′−5′; 4′−5′
D	1−6; 2−6; 2−3; 3−3; 3−8; 7−7; 6−7; 4−5; 5−5; 4−8; 3′−3′; 2′−3′; 3′−8′; 7′−7′; 6′−7′; 2′−6′; 4′−8′; 1′−6′; 5′−5′; 4′−5′
E	5−5; 4−5; 1−6; 2−6; 2−3; 3−3; 3−8; 4−54−8;7−7; 6−7; 4−8; 3′−3′; 2′−3′; 3′−8′; 4′−8′; 7′−7′; 6′−7′; 2′−6′; 4′−8′; 1′−6′; 5′5′; 4′−5′
F	1−6; 2−6; 2−3; 3−3; 3−8; 7−7; 6−7; 4−5; 5−5; 4−8; 3′−3′; 2′−3′; 3′−8′; 7′−7′; 6′−7′; 2′−6′; 4′−8′; 1′−6′; 5′−5′; 4′−5′
G	1−6; 2−6; 6−7; 7−7; 2−3; 3−3; 3−8; 4−5; 5−5; 2′−3′; 3′−3′; 3′−8′; 4′−8′; 4′−5′; 5′−5′; 7′−7; 7′−7; 6′−7′
H	2−3; 3−3; 4−5; 5−5; 6−7; 7−7; 6′−7′; 2′−3′; 5′−5′; 4′−5′; 3′−8′; 3′−3′; 6′−7′; 7′−7′
I	1−6; 2−6; 4−5; 2−3; 3−3; 5−5; 6−7; 7−7; 2′−3′; 3′−3′; 4′−5′; 5′−5′; 8′−4′; 7′−7′; 7′−6′
J	2−3; 3−3; 4−5; 5−5; 6−7; 7−7; 7′−7′; 6′−7′; 3′−3′; 2′−3′; 5′−5′; 4′−5′
K	2−3; 3−3; 4−5; 5−5; 6−7; 7−7; 2′−3′; 3′−3′; 4′−5′; 5′−5′; 6′−7′; 7′−7′
L	2−3; 3−3; 4−5; 5−5; 6−7; 7−7; 2′−3′; 3′−3′; 4′−5′; 5′−5′; 6′−7′; 7′−7′
M	2−3; 3−3; 4−5; 5−5; 6−7; 7−7; 2′−3′; 3′−3′; 4′−5′; 5′−5′; 6′−7′; 7′−7′
N	2−3; 3−3; 4−5; 5−5; 6−7; 7−7; 2′−3′; 3′−3′; 4′−5′; 5′−5′; 6′−7′; 7′−7′
TS1	1−6; 2−6; 2−3; 3−3; 3−8; 7−7; 6−7; 4−5; 5−5; 4−8; 3′−3′; 2′−3′; 3′−8′; 7′−7′; 6′−7′; 2′−6′; 4′−8′; 1′−6′; 5′−5′; 4′−5′
TS2	1−6; 2−6; 2−3; 3−3; 3−8; 7−7; 6−7; 4−5; 5−5; 4−8; 3′−3′; 2′−3′; 3′−8′; 7′−7′; 6′−7′; 2′−6′; 4′−8′; 5′−5′; 4′−5′
TS3	1−6; 2−6; 2−3; 3−3; 3−8; 7−7; 6−7; 4−5; 5−5; 2′−3′; 3′−3′; 3′−8′; 4′−5′; 4′−8′; 5′−5′; 6′−7′; 7′−7′
TS4	1−6; 2−6; 2−3; 3−3; 7−7; 6−7; 4−5; 5−5; 2′−3′; 3′−3′; 3′−8′; 4′−5′; 4′−8′; 5′−5′; 6′−7′; 7′−7′
TS5	2−3; 3−3; 4−5; 5−5; 6−7; 7−7; 2′−3′; 3′−3′; 4′−5′; 5′−5′; 6′−7′; 7′−7′
TS6	2−2; 2−3; 4−5; 5−5; 6−7; 7−7; 2′−2′; 2′−3′; 4′−5′; 5′−5′; 6′−7′; 7′−7′

[a] The cutoff distance for the hydrogen bond is 3.4 Å.

interactions, see Tables 2 and 3 and Figure 2a. The contact also affects the symmetry of the dimer. Two identical molecules can dimerize creating a binary element of symmetry (plane, axis, or inversion center) in their adduct. The existence of the screw axis and of preferential interactions prevents it in 7-PDMA, as is seen in Table 4, where the number of $NH\cdots N_{intra}$ bonds is nine for one strand and 10 for the other.

A slight rearrangement of the inter-strand contacts substitutes some of the hydrogen bonds and the π-stacks to the over-folded configuration, **B**, see Figure 2b, with 20 $NH\cdots N_{intra}$ bonds.

The energy cost of the A→B rearrangement is less than 1 kcal mol^{-1}. This low value comes from a near cancellation between the destabilization of the intermolecular interactions, about 6 kcal mol^{-1}, and the higher stability due to the intra-strand interactions, about −5 kcal mol^{-1}, see Table 1. This is the "entrance" complex of the double helix formation (see below).

A and **B** are only two of the plethora of (low-energy) minima generated by contact of two single helices. These structures lack any intertwined motif and form a dense manifold of "touch and go" complexes. When interacting, the two strands forfeit some of the intrachain energy that is partly compensated by increased interchain interactions. The incipient duplexes differ for the number of π-stacks and NH···N bonds and tend to have high intermolecular destabilization (with a maximum of nearly 14 kcal mol^{-1}) balanced by a lower intramolecular stabilization (with a maximum of nearly −10 kcal mol^{-1}), see **C** to **F**, both in the tables and in Figure 2.

Interconversion of the complexes and equilibria are easily established and take place with low barriers. For instance, Figure 3 illustrates **TS1** that connects adducts **E** to **F** via a barrier of 3.4 kcal mol^{-1}. It also shows **TS2**, which leads to the automerization of **D** through a barrier of 5.1 kcal mol^{-1}. The arrows indicate the motion to reach the nearest local minimum. The connection between minima and transition states was carried out by relaxing the transition state structure and locating the closest stable complexes.

Engaging the Insertion, Phase II, G to I. In this phase, the molecules initiate the double helix formation. Complex **G** is the first structure where the interchain component of the energy is more stabilizing than in **A**. Overall, it is less than 4 kcal mol^{-1} higher in energy than **A**, and is energetically similar to the adducts from **C** to **F**. Although this complex still lacks an intertwined motif, Figure 2 shows that one of the helices is opening to accommodate the end of the other. Importantly, **G** is linked to **B** via **TS3** (Figure 3) that is the transition state with the largest energy located along the reaction pathway. This transition state is unique to the intertwining mechanism and is almost 13 kcal mol^{-1} higher than **A**. The arrows show the bottom end of the green strand and the top end of the yellow chain that edge inside the other molecule. Meanwhile, the opposite ends of the two chains move to make further room in order to enlarge the "entrance" gap. Moreover, the middle parts of the strands, most noticeably the green one, prepare to slide horizontally to find the best interaction with the other chain. The opening of the chain to create this transition state occurs only once in the duplex formation and because of the value of its energy is the overall rate-determining step.

A major slippage occurs after **G**: no minima are found from **G** to **H** and **I**. The latter two supramolecular conformations are generated by a half-turn, screw-in movement. Their energies are still similar to those of the **A** to **F** adducts. However, the intra- and interchain terms that, as before, nearly cancel one other are now about 20 kcal mol^{-1} each. A rather low-lying, 5.4 kcal mol^{-1}, transition state, **TS4**, was located between the "entrance" complex **G** and the first of the two-half-turn duplexes, **H**.

Fast Forward, Phase III, J and K to the Double Helices. A second, even larger, slippage leads to complexes **J** and **K**, also illustrated in the set of figures 2. This time a further full turn of one helix embeds deeply the strands into each other. These structures are already quite close to a full double helix. The stability of **J** and **K** is rather close to that of the initial complex **A**, but about 50 kcal mol^{-1} of intrachain interaction energy is transferred to the interchain one. This is nearly the entire amount of intrachain interaction. It is **TS5**, Figure 3, that connects **I** to **J**, its energy, 10.7 kcal mol^{-1}, is similar, although

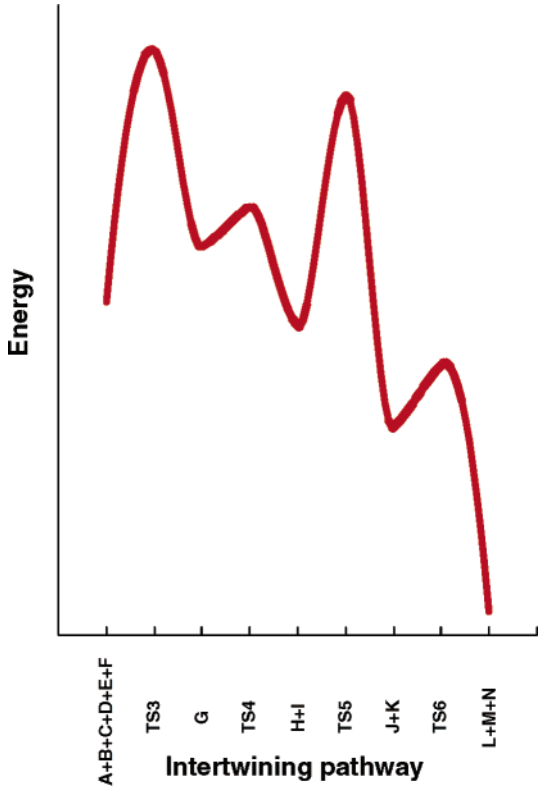

Figure 4. Pictorial summary of the pathway of double helix formation.

slightly less than that of **TS3** that is the transition state that connects the "entrance" complex to the first entwined minima.

While duplexes **J** and **K** are close to the double helix, another partial turn is required to reach it. Adducts **L**, **M**, and **N** are full-fledged double helices. Both **M** and **N** are the lowest energy minima along the entwining pathway. Notice that **M** is the adduct closest to the crystal structure. **TS6** links **K** to **L**, with an energy, -2.1 kcal mol^{-1}, that is even lower than that of the initial back-to-back complexes.

It is noteworthy that only in the region around the final, complete double helices has a larger stability than the contact-complexes of two single helices. Small chemical modifications and/or variation of the solution conditions may slightly disrupt the matching of the strands—which is only achieved at the end of the entwining pathway—and therefore vary greatly the stability of the supramolecular product, a feature that is experimentally observed.[1,2]

Conclusion

The duplex formation is driven by a series of slippage steps. A few energy barriers, or transition states, exist between the stable intermediates that include (1) back-to-back complexes, **A**−**F**, (2) the adduct of the initial insertion, **G**, (3) half-turn screw-in conformers, **H** and **I**, (4) one-and-half-turn screw-in duplexes, **J** and **K**, and (5) double helices, **L**, **M**, **N**.

Pictorially, the pathway is a series of roller-coasting hills all the way to the duplex, with the largest one met at the beginning, see Figure 4 for a summary. As one strand winds its way entwining with the other, the intramolecular non bonding interactions of the initial minimum are replaced by new and more numerous supramolecular ones.

Slippage mechanisms have been found before in supramolecular chemistry, for instance for the formation of rotaxanes,[8] dendrimers,[9] in organometallic chemistry,[10] and even in all-carbon peapods where the molecular translational motion of C_{60} is nearly diffusional, since breaking of a π interaction between a nanotube and C_{60} immediately creates a new one,[11] in a way similar to what occurs in PDMA, where both hydrogen bonds and π-stacks compete and exchange continuously along the pathway to provide the scenario presented in this work.

JA038103F

(8) (a) Raymo, F. M.; Houk, K. N.; Stoddart, J. F. *J. Am. Chem. Soc.* **1998**, *120*, 9318. (b) Fujita, M.; Ibukuro, F.; Ogura, K.; Seki, H.; Kamo, O.; Imanari, M. *J. Am. Chem. Soc.* **1996**, *118*, 899. (c) Macartney, D. H. *J. Chem. Soc., Perkin Trans.* **1996**, *12*, 2775.
(9) Elizarov, A. M.; Chang, T.; Chiu, S.-H.; Stoddart, J. F. *Org. Lett.* **2002**, *4*, 3565.
(10) Mizuta, T.; Imamura, Y.; Miyoshi, K. *J. Am. Chem. Soc.* **2003**, *125*, 2068.
(11) Melle-Franco, M.; Kuzmany, H.; Zerbetto, F. *J. Phys. Chem. B* **2003**, *107*, 6986.